Analytical kinetic model of native tandem promoters in *E. coli*

Vatsala Chauhan[1¶], Mohamed N.M. Bahrudeen[1¶], Cristina S.D. Palma[1], Ines S.C. Baptista[1], Bilena L.B. Almeida[1], Suchintak Dash[1], Vinodh Kandavalli[2], and Andre S. Ribeiro[1*]

[1] Laboratory of Biosystem Dynamics, Faculty of Medicine and Health Technology, Tampere

University, Finland.

[2] Department of Cell and Molecular Biology, Uppsala University, Uppsala, Sweden.

[*] Corresponding author. E-mail: andre.sanchesribeiro@tuni.fi

[¶] These authors contributed equally to this work.

Abstract

Closely spaced promoters in tandem formation are abundant in bacteria. We investigated the evolutionary conservation, biological functions, and the RNA and single-cell protein expression of genes regulated by tandem promoters in *E. coli*. We also studied the sequence (distance between transcription start sites 'd_{TSS}', pause sequences, and distances from oriC) and potential influence of the input transcription factors of these promoters. From this, we propose an analytical model of gene expression based on measured expression dynamics, where RNAP-promoter occupancy times and d_{TSS} are the key regulators of transcription interference due to TSS occlusion by RNAP at one of the promoters (when $d_{TSS} \leq 35$ bp) and RNAP occupancy of the downstream promoter (when $d_{TSS} > 35$ bp). Occlusion and downstream promoter occupancy are modeled as linear functions of occupancy time, while the influence of d_{TSS} is implemented by a continuous step function, fit to *in vivo* data on mean single-cell protein numbers of 30 natural genes controlled by tandem promoters. The best-fitting step is at 35 bp, matching the length of DNA occupied by RNAP in the open complex formation. This model accurately predicts the squared coefficient of variation and skewness of the natural single-cell protein numbers as a function of d_{TSS}. Additional predictions suggest that promoters in tandem formation can cover a wide range of transcription dynamics within realistic intervals of parameter values. By accurately capturing the dynamics of these promoters, this model can be helpful to predict the dynamics of new promoters and contribute to the expansion of the repertoire of expression dynamics available to synthetic genetic constructs.

Author Summary

Tandem promoters are common in nature, but investigations on their dynamics have so far largely relied on synthetic constructs. Thus, their regulation and potentially unique dynamics remain unexplored. We first

1

32   performed a comprehensive exploration of the conservation of genes regulated by these promoters in *E.*

33   *coli* and the properties of their input transcription factors. We then measured protein and RNA levels

34   expressed by 30 *Escherichia coli* tandem promoters, to establish an analytical model of the expression

35   dynamics of genes controlled by such promoters. We show that start site occlusion and downstream RNAP

36   occupancy can be realistically captured by a model with RNAP binding affinity, the time length of open

37   complex formation, and the nucleotide distance between transcription start sites. This study contributes to

38   a better understanding of the unique dynamics tandem promoters can bring to the dynamics of gene

39   networks and will assist in their use in synthetic genetic circuits.

Introduction

41   Closely spaced promoters exist in all branches of life in convergent, divergent, and tandem formations [1-

42   7]. Models of tandem promoters [8-10] have largely been based on measurements of synthetic constructs

43   [11-13] and predict that such promoter arrangements result in unique transcription dynamics due to the

44   interference between RNAPs transcribing the promoters [9, 10, 14-19].

45   When an RNAP is committed to form the open complex (OC), a process lasting up to hundreds of seconds

46   [20-22], it occupies approximately 35 base pairs (bp), from the transcription start site (TSS, position 0) until

47   position -35 [23- 25]. If the TSS of a neighbouring promoter is closer than 35 bp away, it will not be possible

48   for both promoters to be occupied simultaneously, since an RNAP occupying one of them will 'occlude' the

49   other, preventing it from being reached [9]. However, if the promoters are more than 35 bp apart, this

50   occlusion does not occur. Instead, interference will occur when RNAPs elongating from the upstream

51   promoter collide with an RNAP occupying the downstream promoter [14] (in either closed or open complex

52   formation), forcing one of the RNAPs to fall-off (both scenarios are likely possible, and we expect it to differ

53   with, e.g., the binding affinity of the RNAP to the downstream promoter). Meanwhile, models based on

54   empirical parameter values suggest that collisions between two elongating RNAPs are rare (because

55   events such as pausing or simultaneous initiations from both promoters are rare). Also, even if and when

56   such collisions occur, they are unlikely to result in fall-offs since the RNAPs are moving at similar speeds

57   and in the same direction [9][10][26].

58   Models suggest that both forms of interference decrease the mean RNA production rate while increasing

59   its noise based on the distance between promoters (d_{TSS}), their strengths [10], and the time spent between

60   commitment of the RNAP to OC and escape from the promoter region [27]. These hypotheses have yet to

61   be empirically validated in natural tandem promoters.

62   We studied how d_{TSS} and the time spent by RNAPs on the TSSs affect gene expression dynamics due to

63   interference between the transcription processes of tandem promoters (Fig 1). We consider only the natural

64   tandem promoters that neither overlap with nor have in between another gene (positionings I and II, which

65   differ in if the promoter regions overlap or not) (see the other arrangements in Fig. S1 in the S2 Appendix).

66   The numbers of these arrangements in *E. coli* are shown in Table S8 in the S3 Appendix. From the
67   measurements of these genes' protein levels, we then establish a model that we use to explore the state
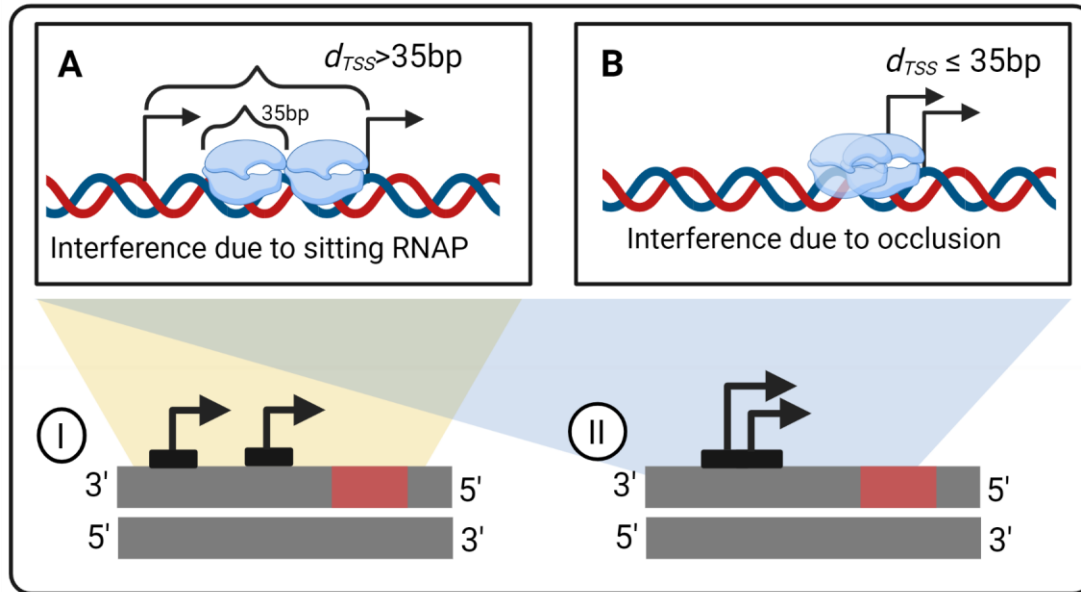68   space of potential dynamics under the control of tandem promoters (Fig 2 illustrates our workflow).

69
70   **Fig 1. Interference between tandem promoters with different arrangements relative to each other
71   and to neighbour genes. (A)** Interference by an RNAP occupying the downstream promoter on the activity
72   of the elongating RNAP from upstream promoter. The TSSs need to be at least 36 bp apart (the length
73   occupied by an RNAP when in OC, [23, 25]) **(B)** Interference by occlusion of one of the promoter's TSS by
74   an RNAP on the TSS of the other promoter. The distance between the TSSs need to be ≤ 35 bp apart. Blue
75   clouds are RNAPs. Black arrows sit on TSSs and point towards the direction of transcription elongation.
76   Arrangements **(I-II)** of two promoters studied in the manuscript in tandem formation are represented. The
77   red rectangles are the protein coding regions. We studied only the natural tandem promoters that neither
78   overlap with nor have in between another gene (arrangements I and II, which differ based on whether the
79   promoter regions overlap or not). Other arrangements (not considered in this study) are shown in Fig. S1
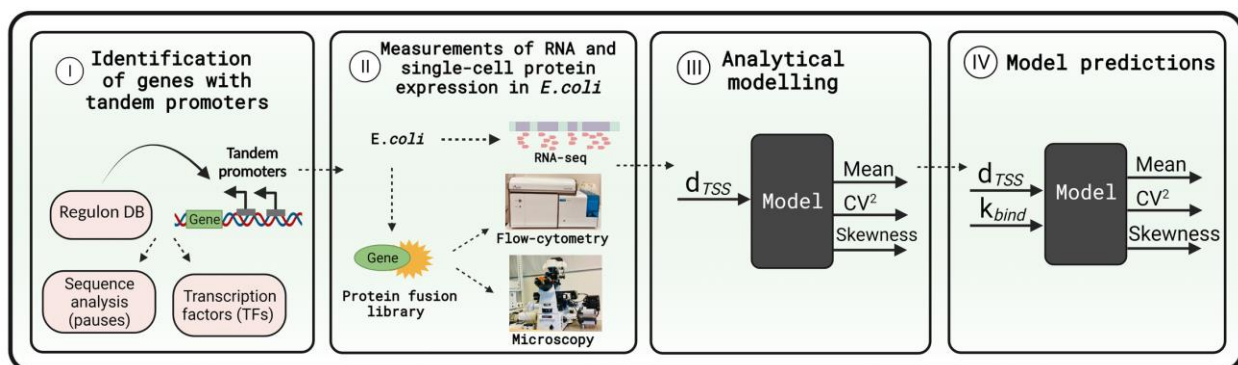80   in the S2 Appendix. Figure created with BioRender.com.

81

82

3

83   **Fig 2. Workflow.** (I) We identified genes controlled by tandem promoters in Regulon DB. (II) Next, we
84   measured the single-cell protein levels of those genes with arrangements I and II that are tagged in the
85   YFP strain library [28]. We also measured the mean RNA fold changes of these genes over time (S1
86   Appendix, section 'RNA-seq measurements and data analysis'). (III) We used the single-cell data to tune
87   the model. (IV) Finally, we used the model to explore the state space of protein expression. Figure created
88   with BioRender.com.

Results

90   *E. coli* has 831 genes controlled by two or more promoters in tandem formation (RegulonDB and section
91   'Selection of natural genes controlled by tandem promoters for flow-cytometry' in the S1 Appendix).
92   However, to study the dynamics of genes controlled by tandem promoters, we focused on only 102 of them,
93   because their activity is expected to be undisturbed by neighboring genes in the DNA (arrangements I and
94   II in Fig 1), for reasons described in section 'Selection of natural genes controlled by tandem promoters for
95   flow-cytometry' in the S1 Appendix.

96   Further, these promoters do not have specific short nucleotide sequences capable of affecting RNAP
97   elongation (section 'Pause sequences' in the S4 Appendix). Also, the 102 genes expressed by these
98   promoters are not overrepresented in a particular biological process (section 'Over-representation test' in
99   the S4 Appendix). From time-lapse RNA-seq data (S1 Appendix, section 'RNA-seq measurements and
100 data analysis'), we also did not find evidence that their dynamics are affected by their input transcription
101 factors (TFs) in our measurement conditions (section 'Input-output transcription factor relationships' in the
102 S4 Appendix) nor by H-NS in a consistent manner (section 'Regulation by H-NS' in the S4 Appendix).
103 Finally, they do not exhibit any particular TF network features (Table S3 in the S3 Appendix). As such,
104 neither input TFs nor specific nucleotide sequences are considered in the model below. In addition to all of
105 the above, we found no correlations between the shortest distance from the TSS of upstream promoters
106 from the $oriC$ region in the DNA and expression levels (section 'Relationship with the $oriC$ region' in the
107 S4 Appendix).

Model of gene expression controlled by tandem promoters

109 RNAPs bind, slide along, and unbind from a promoter several times until, eventually, one of them finds the
110 TSS [29-30], commits to OC at the TSS, and initiates transcription elongation.

111 Reactions (1a1) are a 4-step (I-IV) model of transcription [20, 31]. The forward reaction in step I in (1a1)
112 models RNAP binding to a free promoter (P_{free}), which becomes no longer free albeit the RNAP might not
113 yet have reached the TSS. This state, pre-finding of the TSS, is here named P_{bound} and its occurrence
114 increases with RNAP concentration, $[R]$. Next, as it percolates the DNA, the RNAP should find and stop at

115   the nearest TSS and form a closed complex (CC) with the DNA (step II, Reaction 1a1). CCs are unstable,

116   i.e. reversible [22] (reaction 1a2) but, eventually, one of them will commit to OC irreversibly [32], via step

117   III, Reaction 1a1 [21-22]. It follows RNAP escape from the TSS, freeing the promoter (step IV, Reaction

118   1a1) [33-37]. Then, the RNAP elongates (R_{elong}) until producing a complete RNA (reaction 1a3) and freeing

119   itself.

120   These set of reactions usually model well stochastic transcription dynamics [20]. However, if two promoters

121   are closely spaced in tandem formation, they can interfere [38]. Figure 3 shows sequences of events that

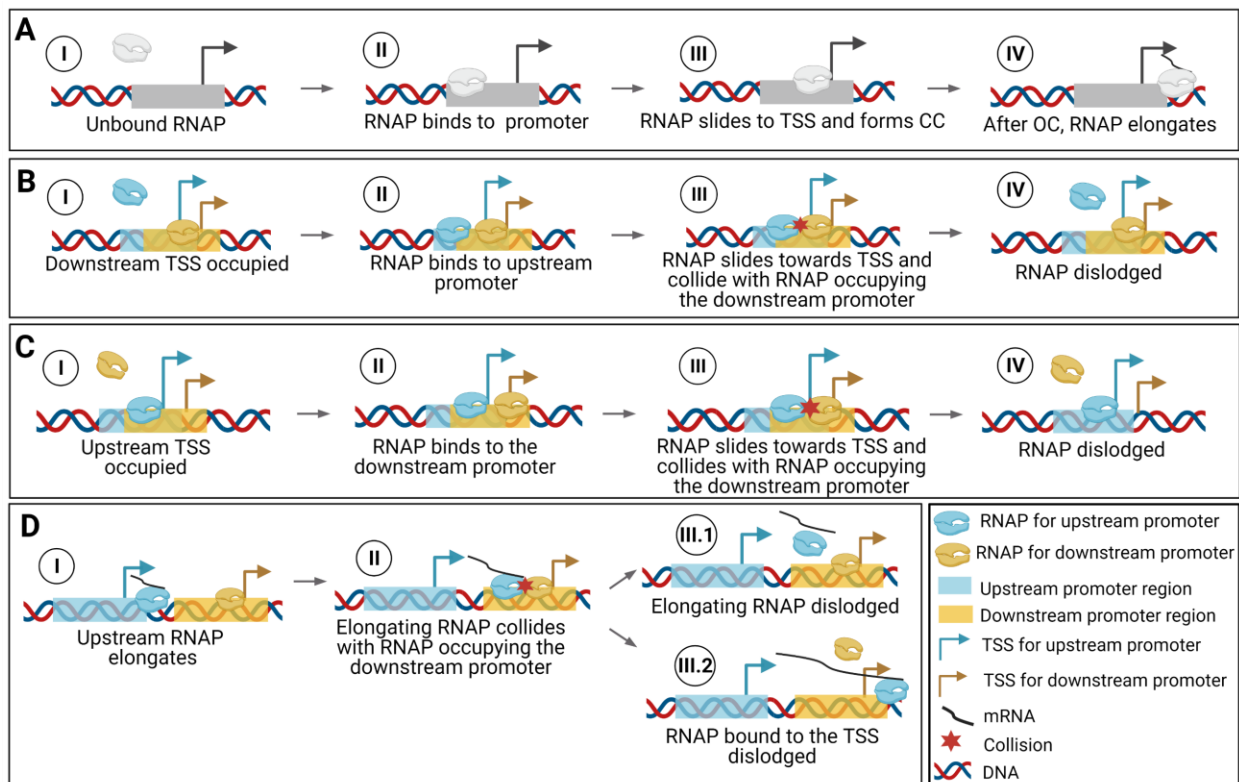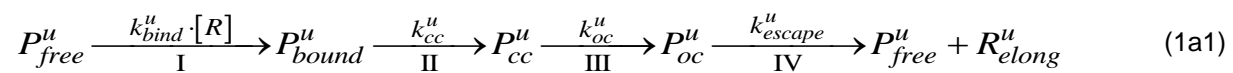122   can lead to interference between tandem promoters, not accounted for by the model above.

123

124   **Fig 3**. **Events leading to transcriptional interference between tandem promoters**. (**A**) Sequence of

125   events in transcription in isolated promoters. A similar set of events occurs in tandem promoters, if only one

126   RNAP interacts with them at any given time. (**B / C**) Interference due to the occlusion of the *downstream* /

127   *upstream* promoter by a bound RNAP, which will impede the incoming RNAP from binding to the TSS. (**D**)

128   Interference of the activity of the RNAP incoming from the upstream promoter by the RNAP occupying the

129   downstream promoter. One of these RNAPs will be dislodged by the collision. Created with BioRender.com.

130   From Figure 3, if the TSSs are sufficiently close, the occupancy of one TSS by an RNAP will occlude the

131   other TSS, blocking its kinetics [18]. This is accounted for by reaction 1a5, which competes with CC

132   formation in reaction 1a1. Its rate constant, $k_{occlusion}$, is defined in the next section. In (1a5), 'u/d' stands for

133   occlusion of the upstream promoter by an RNAP on the TSS of the downstream promoter.
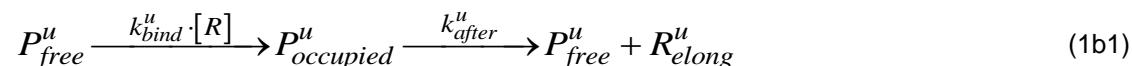
134 Instead, if the TSSs are not sufficiently close, they will still interfere since the elongating RNAP (R_{elong})

135 starting from the upstream promoter can collide with RNAPs on the TSS of the downstream promoter. This

136 can dislodge either RNAP via (reaction 1a4) or (reaction 2a3), depending on the sequence-dependent

137 binding strength of the RNAP to the TSS [9].

138 Finally, once reaction 1a1 occurs, either reaction 1a3 or 1a4 occur. To tune their competition, we introduced

139 the terms ω_d and (1-ω_d) in their rate constants, with ω_d being the fraction of times that an elongating RNAP

140 from an upstream promoter finds an RNAP occupying the downstream promoter. Meanwhile, 'f' is the

141 fraction of times that the RNAP occupying the downstream promoter falls-off due to the collision with an

142 elongating RNAP, whereas '1-f' is the fraction of times that it is the elongating RNAP that falls-off.
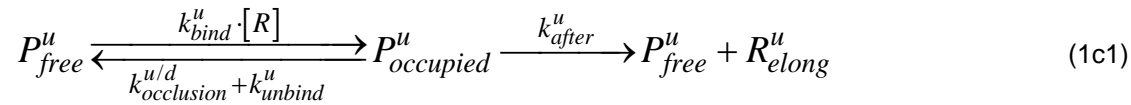
143
$$P^u_{free} \xrightarrow[\text{I}]{k^u_{bind} \cdot [R]} P^u_{bound} \xrightarrow[\text{II}]{k^u_{cc}} P^u_{cc} \xrightarrow[\text{III}]{k^u_{oc}} P^u_{oc} \xrightarrow[\text{IV}]{k^u_{escape}} P^u_{free} + R^u_{elong} \qquad (1a1)$$

144
$$P^u_{cc} \xrightarrow{k_{unbind}} P^u_{free} \qquad (1a2)$$

145
$$R^u_{elong} \xrightarrow{k^u_{elong} \cdot \left(1 - \omega_d \cdot f\right)} RNA \qquad (1a3)$$

146
$$R^u_{elong} \xrightarrow{k^u_{elong} \cdot \omega_d \cdot f} \varnothing \qquad (1a4)$$

147
$$P^u_{bound} \xrightarrow{k^{u/d}_{occlusion}} P^u_{free} \qquad (1a5)$$

148 Next, we reduced the model and derived its analytical solution. First, since P_{cc} completion is expected to

149 be faster than P_{bound} completion ([10] and references within) we merged them into a single state, $P_{occupied}$,

150 which represents a promoter occupied by an RNAP prior to commitment to OC, whose time length is similar

151 to P_{bound}.

152 Similarly, in standard growth conditions, the occurrence of multiple failures in escaping the promoter [46]

153 per OC completion should only occur in promoters with the highest binding affinity to RNAP. Thus, in

154 general promoter escape should be faster than OC [20, 32]. We thus merged OC and promoter escape into

155 one step named 'events *after* commitment to OC', with a rate constant k_{after}. The simplified model is thus:

156
$$P^u_{free} \xrightarrow{k^u_{bind} \cdot [R]} P^u_{occupied} \xrightarrow{k^u_{after}} P^u_{free} + R^u_{elong} \qquad (1b1)$$
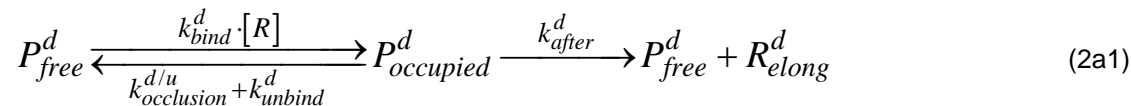
157 These two steps are not merged since only the first differs with RNAP concentration [20, 26,39]. Further,

158 reports [40-41] indicate that *E. coli* has ~100-1000 RNAPs free for binding at any moment but ~4000 genes,

159 suggesting that the number of free RNAPs is a limiting factor.

6

160 Finally, we merge (1a2), (1a5) and (1b1) in one multistep without affecting the model kinetics:

161
$$P_{free}^u \xleftrightarrow[k_{occlusion}^{u/d}+k_{unbind}^u]{k_{bind}^u \cdot [R]} P_{occupied}^u \xrightarrow{k_{after}^u} P_{free}^u + R_{elong}^u \qquad (1c1)$$

162 Overall, this reduced model of transcription of upstream promoters has a multistep reaction of transcription
163 initiation (1c1), a reaction of transcription elongation (1a3) and a reaction for failed elongation due to RNAPs
164 occupying the downstream promoter (1a4).

165 Regarding RNA production from the downstream promoter, it should either be affected by occlusion if d_{TSS}
166 ≤ 35, or by RNAPs elongating from the upstream promoter if d_{TSS} > 35 (Fig 3). We thus use reactions (2a1),
167 (2a2), and (2a3) to model these promoters' kinetics:

168
$$P_{free}^d \xleftrightarrow[k_{occlusion}^{d/u}+k_{unbind}^d]{k_{bind}^d \cdot [R]} P_{occupied}^d \xrightarrow{k_{after}^d} P_{free}^d + R_{elong}^d \qquad (2a1)$$

169
$$R_{elong}^d \xrightarrow{k_{elong}^d} RNA \qquad (2a2)$$

170
$$P_{free}^d \xrightarrow{k_{occupy}} P_{occupied}^d \qquad (2a3)$$

171 Finally, one needs to include a reaction for translation (reaction 3), as a first order process since protein
172 numbers follow RNA numbers linearly (Fig S6 in the S2 Appendix), and reactions for RNA and protein
173 decay accounting for degradation and for dilution due to cell division (reactions 4a and 4b, respectively).
174 TF regulation is not included as noted above (Figs S3 and S4A in the S2 Appendix).

175
$$RNA \xrightarrow{k_p} Prot \qquad (3)$$

176
$$RNA \xrightarrow{k_{rd}} \varnothing \qquad (4a)$$

177
$$Prot \xrightarrow{k_{pd}} \varnothing \qquad (4b)$$

Transcription interference by occlusion

179 In a pair of tandem promoters, the $k_{occlusion}$ of one of them should increase with the fraction of time that
180 the other one is occupied. Further, it should decrease with increasing d_{TSS} between the two promoters'

181   TSS. We thus define $k_{occlusion}$ for the upstream (Eq. 5a) and downstream (Eq. 5b) promoters, respectively

182   as:

183    $$k_{occlusion}^{u/d} = k_{ocl}^{max} \cdot I(d_{TSS}) \cdot \omega_d \qquad \text{(5a)}$$

184    $$k_{occlusion}^{d/u} = k_{ocl}^{max} \cdot I(d_{TSS}) \cdot \omega_u \qquad \text{(5b)}$$

185   Here, k_{ocl}^{max} is the maximum occlusion possible. It occurs when the two TSSs completely overlap each other

186   ($d_{TSS} = 0$) *and* the TSS of the 'other' promoter is always occupied. Meanwhile, $I(d_{TSS})$ models distance-

187   dependent interference.

188   We tested four models of interference: 'exponential 1', 'exponential 2', 'step', and 'zero order' (Table 1).

189   The first two assume that the effects of occlusion decrease exponentially with d_{TSS} (first and second order

190   dependency, respectively).

191   Meanwhile, the 'Step' model assumes that interference only occurs precisely in the region in the DNA

192   occupied by the RNAP when in OC formation. For this, it uses a logistic equation to build a continuous step

193   function, where L is the length of DNA (in bp) occupied by the RNAP in OC. As such, L tunes at what d_{TSS}

194   the step occurs, while m is the steepness of that step (set to 1 bp^{-1}).

195   Finally, the 'Zero order' model assumes (unrealistically) that interference by occlusion, is independent of

196   d_{TSS}. Fig S7 in the S2 Appendix shows how $k_{occlusion}$ differs with d_{TSS} in each model, for various

197   parameter values.

198   **Table 1**. **Potential models of transcriptional interference due to promoter occlusion considered.**

Interference by occlusion	$I(d_{TSS})$	$k_{occlusion}$
Exponential 1 ("Exp1")	$e^{-(b_1 \cdot d_{TSS})}$	$k_{ocl}^{max} \cdot e^{-(b_1 \cdot d_{TSS})} \cdot \omega$
Exponential 2 ("Exp2")	$e^{-(b_1 \cdot d_{TSS} + b_2 \cdot d_{TSS}^2)}$	$k_{ocl}^{max} \cdot e^{-(b_1 \cdot d_{TSS} + b_2 \cdot d_{TSS}^2)} \cdot \omega$
Step ("Step")	$1 - \dfrac{1}{1 + e^{-m \cdot (d_{TSS} - L)}}$	$k_{ocl}^{max} \cdot \left(1 - \dfrac{1}{1 + e^{-(d_{TSS} - L)}}\right) \cdot \omega$, for m = 1 bp^{-1}

Zero order ("ZeroO")	k	$k_{ocl}^{max} \cdot \omega$

199

200   Finally, ω is the fraction of time that the 'other' promoter is occupied. It ranges from 0 (no occupancy) to 1

201   (always occupied). It is estimated for upstream and downstream promoters as:

$$\omega_u = \frac{k_{bind}^u \cdot [R]}{k_{unbind}^u + k_{bind}^u \cdot [R] + k_{after}^u} \tag{6a}$$

202

$$\omega_d = \frac{k_{bind}^d \cdot [R]}{k_{unbind}^d + k_{bind}^d \cdot [R] + k_{after}^d} \tag{6b}$$

203

204   Similarly, if k_{occupy}^{max} is the maximum possible interference due to RNAPs occupying the downstream

205   promoter, k_{occupy} is defined as:

$$k_{occupy} = \omega_u \cdot k_{after} \cdot k_{occupy}^{max} \cdot (1-f) \tag{7}$$

206

Analytical solution of the moments of the single-cell protein numbers

209   Next, we derived an analytical solution of the expected mean single-cell protein numbers at steady state,

210   M_P, which is later tuned to fit the empirical data. For any gene, regardless of the underlying kinetics of

211   transcription, k_r is the *effective* rate of RNA production. Based on the reactions above, the mean protein

212   numbers in steady state will be (see sections "Analytical model of mean RNA levels controlled by a single

213   promoter in the absence of a closely spaced promoter" and "Derivation of mean protein numbers at steady

214   state produced by a pair of tandem promoters" in the S1 Appendix):

$$M_P = \frac{k_r \cdot k_p}{k_{rd} \cdot k_{pd}} \tag{8}$$

215

216   This equation applies to a pair of tandem promoters as well. In that case, assuming that k_{bind} of the two

217   tandem promoters is similar, we have:

218
$$k_r = \left(\dfrac{\dfrac{k_{bind} \cdot [R] \times k_{after} \cdot (1 - \omega_d \cdot f)}{k_{occlusion} + k_{bind} \cdot [R] + k_{unbind} + k_{after}} +}{\dfrac{k_{bind} \cdot [R] \times k_{after}}{k_{occlusion} + k_{occupy} + k_{bind} \cdot [R] + k_{unbind} + k_{after}}} \right)$$
(9)

219   To derive the other moments, we considered that empirical single-cell protein numbers in *E. coli* are well fit

220   by negative binomials [28]. Consequently, M_p and the squared coefficient of variation CV_P^2, should be

221   related as (Equations S28 to S38 in the S1 Appendix):

222    $$\log_{10}\left(CV_P^2\right) = \log_{10}(C_1) - \log_{10}\left(M_P\right), \qquad \text{with} \qquad C_1 = \frac{k_p}{k_{pd} + k_{rd}}$$
(10)

223   This relationship matches empirical data at the genome wide level, except for genes with high transcription

224   rates [54]. Additionally, we further derived a relationship (Section 'CV^2 and Skewness of single-cell protein

225   expression of a tandem promoter's model' in the S1 Appendix) between M_P and the skewness, S_P, of the

226   single-cell distribution of protein numbers:

227    $$\log_{10}\left(S_P\right) = \log_{10}\left(C_2\right) - \frac{1}{2} \cdot \log_{10}\left(M_P\right), \qquad \text{with} \qquad C_2 = 2\sqrt{C_1} - \frac{1}{\sqrt{C_1}}$$
(11)

Single-cell distributions of protein numbers

229   To validate the model, we measured by flow-cytometry the single-cell distributions of protein fluorescence

230   of 30 out of the 102 genes known to be controlled by tandem promoters (with arrangements I and II).

231   Measurements were made in 1X and 0.5X media (3 replicates per condition) using cells from the YFP strain

232   library (section 'Strains and Growth Conditions' in the S1 Appendix). Data from past studies show that, in

233   these 30 genes, RNA and protein numbers are well correlated (Fig S6 in the S2 Appendix) in standard

234   growth conditions. Past studies also suggest that most of these genes are active during exponential growth

235   (~95% of our 30 genes selected should be active, according to data in [42] using SEnd-seq technology).

236   Single-cell distributions of protein expression levels are shown in Fig 4A for one of these genes as an

237   example. The raw data from all 30 genes (only one replicate) are shown in Fig S8 in the S2 Appendix.

238   Finally, the mean, CV^2 and skewness for each gene, obtained from the triplicates, are shown in Excel

239   sheets 1 and 2 in the S6 Table. In addition, we also show this mean, CV^2 and skewness after subtracting

240   the first, second, and third moments of the single-cell distribution of the fluorescence of control cells, which

241   do not express YFP (Sheets 3, 4 in the S6 Table) (Section 'Subtraction of background fluorescence from

242   the total protein fluorescence' in the S1 Appendix).

243   Based on the analysis of the data of these 30 genes, we removed from subsequent analysis those genes

244   (5 in 1X and 14 in 0.5X) whose mean, variance, or third moment of their protein fluorescence distributions

245   are lower than in control cells (not expressing YFP), i.e., than cellular autofluorescence (Sheets 3, 4 in S6

246   Table). As such, only one gene studied here (in condition 1X alone) codes for a protein that is associated

247   to membrane-related processes, which might affect its quantification (section 'Proteins with membrane-

248   related positionings' in S4 Appendix). As such, we do not expect this phenomenon to influence our results

249   significantly. The data from these genes removed from further analysis is shown in Fig S6 in S2 Appendix

250   alone, for illustrative purposes.

251   We started by testing the accuracy of the background-subtracted flow-cytometry data by confronting it with

252   microscopy data (also after background subtraction, see section 'Microscopy and Image Analysis' in the S1

253   Appendix). We collected microscopy data on 10 out of the 30 genes (Table S7 in the S3 Appendix). The

254   microscopy measurements of the mean single-cell fluorescence expressed by these genes (example image

255   in Fig. 4B), were consistent, statistically, with the corresponding data obtained by flow-cytometry (Fig 4C).

256   Next, we converted the fluorescence distributions from flow-cytometry (25 genes in 1X and 16 genes in

257   0.5X) into protein number distributions. In Fig 4D we plotted our measurements of mean protein

258   fluorescence in 1X against the protein numbers reported in [28] for the same genes, in order to obtain a

259   scaling factor (sf = 0.09). Using sf, we estimated M_P, CV_P^2, and S_P of the distribution of protein numbers

260   expressed by the tandem promoters in (Sheets 5, 6 in S6 Table) (Section 'Conversion of protein

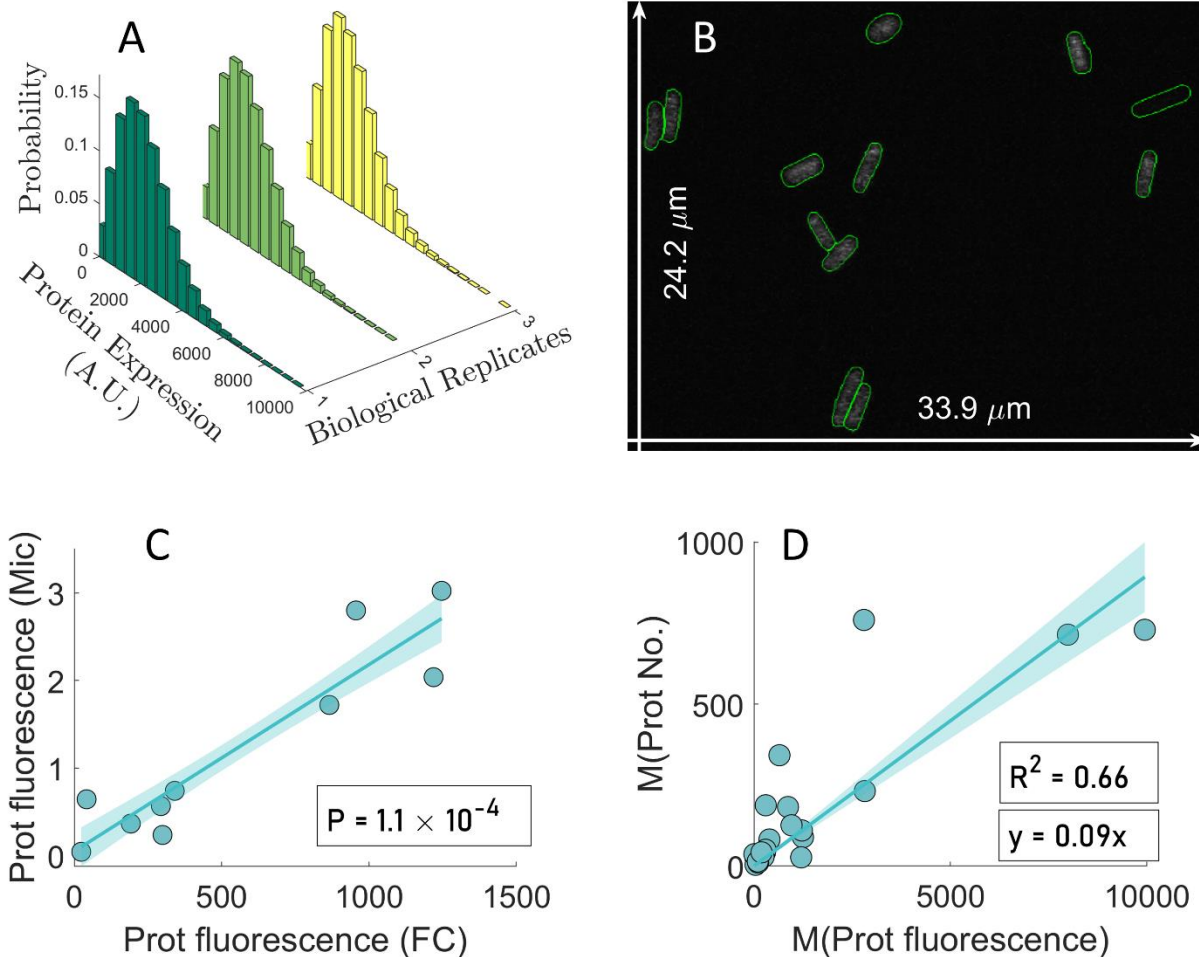261   fluorescence to protein numbers' in S1 Appendix).

Fig 4. Single cell protein numbers by microscopy and flow-cytometry. (A) Example single-cell distributions (3 biological replicates) of fluorescence (in arbitrary units) of cells with a YFP tagged gene controlled by a pair of tandem promoters obtained by flow-cytometry, 'FC'. (B) Example confocal microscopy image of cells overlapped by the results of cell segmentation from the corresponding phase contrast image. The two white arrows show the dimensions of the image, for scaling purposes. (C) Mean single-cell protein fluorescence of 10 genes (Table S7 in the S3 Appendix) when obtained by FC plotted against when obtained by microscopy, 'Mic'. (D) Mean single-cell protein fluorescence (own measurements) plotted against the corresponding mean single-cell protein numbers reported in [28]. From the equation of the best fitting line without y-intercept (y-intercept = 0), we obtained a scaling factor, *sf,* equal to 0.09.

To test the robustness of the estimation of the scaling factor, we also estimated a scaling factor from 10 other genes present in the YFP strain library [28] (listed in Table S2 in S3 Appendix). These genes were selected as described in the section 'Selection of natural genes controlled by single promoters' in S1 Appendix. Using the data from this new gene cohort (Supplementary Figure S9A in S2 Appendix) reported in S7 Table, we estimated a scaling factor of 0.08, supporting the previous result. Meanwhile, since when

277 merging the data from tandem and single promoters, the resulting scaling factor equals 0.09
278 (Supplementary Figure S9B in S2 Appendix), we opted for using 0.09 from here onwards.

279 We also tested how sensitive the estimated scaling factor is to the removal of data points. Specifically, for
280 1000 times, we discarded N randomly selected data points, and estimated the resulting scaling factor. We
281 then compared, for each N, the mean and the median of the distribution of 1000 scaling factors
282 (Supplementary Figure S10 in S2 Appendix). Since the median is not sensitive to outliers, if mean and
283 median are similar, one can conclude that the scaling factor is not biased by a few data points. Visibly, the
284 mean and the median only start differing for N larger than 6, which corresponds to nearly 30% of the data.

Log-log relationship between the mean single-cell protein numbers of tandem promoters and the other moments

287 We plotted M_P against CV_P^2 and S_P in log-log plots, in search for the fitting parameters, 'C_1' and 'C_2', to
288 estimate the rate of protein production per RNA (equation 10). To increase the state space covered by our
289 measurements, in addition to M9 media (named '1X'), we also used diluted M9 media (named '0.5X'),
290 known to cause cells to have lower RNAP concentrations (Fig. 5A) (Section 'Strains and growth conditions'
291 in the S1 Appendix), without altering the division rate (Figs. S11A and S11B in the S2 Appendix). We note
292 that 1X and 0.5X only refer to the degree of dilution of the original media and not to how much RNAP
293 concentration and consequently, protein concentrations, were reduced by media dilution. From the same
294 figures, we attempted stronger dilutions, but no further decreases in RNAP concentration were observed
295 and the growth rate decreased.

296 Next, from Fig 5B, most genes (of those expressing tangibly in both media) suffered similar reductions (well
297 fit by a line) in protein numbers with the media dilution, as expected by the model of gene expression
298 (Equations 8 and 9). This linear relationship could also be interpreted as evidence that the difference in
299 expression of these genes between the two conditions is not affected by TFs in our measurement
300 conditions. Namely, if TF influences existed, and TF numbers changed, they would likely be diversely
301 affected by their output genes (weakly and strongly activated, repressed, etc.) and, thus, our proteins of
302 interest would not have changed in such similar manners (linearly).

303 Meanwhile, as in [44-45], CV_P^2 decreases linearly with M_P (log-log scale), irrespective of media ($R^2 > 0.8$
304 in all fitted lines), in agreement with the model (Fig 5C). Fitting Equation 10 to the data, we extracted C_1 in
305 each condition. S_P also decreases linearly with M_P, irrespective of the media (Fig 5D). Similar to above,
306 Equation 11 was fitted to each data set and C_1 and C_2 were obtained ($R^2 > 0.6$ for all lines).

13

307 Since C_1 from Fig 5C and 5D differed slightly (likely due to noise), we instead obtained C_1 and C_2 values

308 that maximized the mean R^2 of both plots. Using 'fminsearch' function in MATLAB [46], we obtained C_1 =

309 72.71 and C_2 = 16.94 (R^2 of 0.80 and 0.61, respectively) for Fig 5C and Fig 5D, respectively.
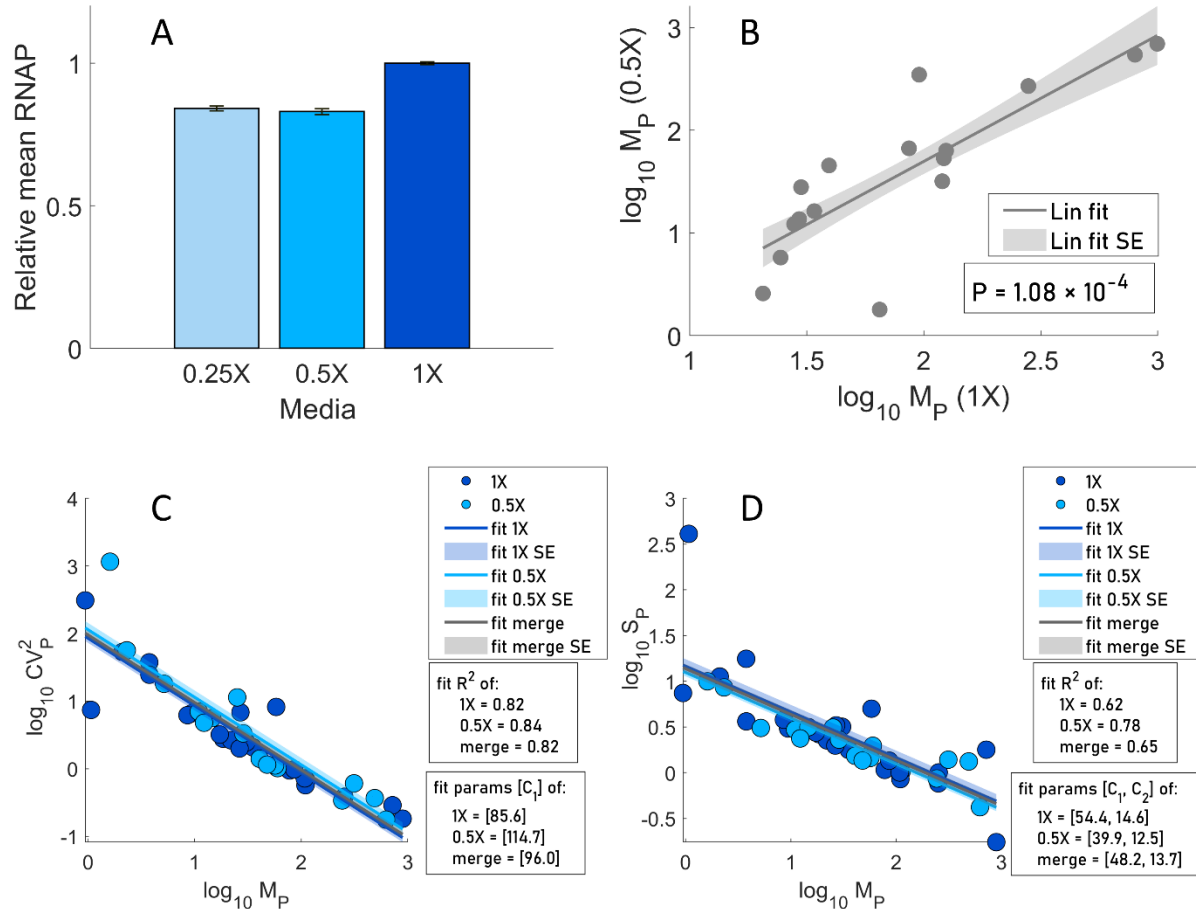

310

Fig 5. Relative RNAP concentrations along with the relationships between the moments of the single cell distributions of protein numbers. (A) Relative RNAP levels measured by flow-cytometry (Section 'flow-cytometry' in the S1 Appendix) in three media. (B) Scatter plot between M_P in M9 (1X) and diluted M9 (0.5X) media. Also shown are the best fitting line and standard error and p-value for the null hypothesis that the slope is zero. (C) M_P vs CV_P^2 and (D) M_P vs S_P of single-cell protein numbers of genes with tandem promoters in M9 (1X) and M9 diluted (0.5X) media. The lines and their shades are the best fitting lines and standard errors, respectively. 'Merge' stands for data from both 0.5X and 1X conditions.

Inference of parameter values and model predictions as a function of d_{TSS}

14

320   We next used the model, after fitting, to predict how d_{TSS} and the promoters' occupancy regulate the

321   moments of the single-cell distribution of protein numbers (M_P, CV_P^2, and S_P) under the control of tandem

322   promoters. We started by assuming the parameter values from the literature listed in Table 2 and tuned the

323   remaining parameters.

324   To set the RNAP numbers in Table 2, we considered that the RNAPs affecting transcription rates are the

325   *free* RNAPs in the cell, and that, for doubling times of 30 min in rich medium, there are ~1000 free RNAPs

326   per cell [41]. Meanwhile, for doubling times of 60 min in minimal medium, there are ~144 [40]. In both our

327   media, we observed a doubling time of ~115 mins (Fig. 5B). Thus, we expect the free RNAP in 1X to also

328   be ~144/cell or lower. Meanwhile, in 0.5X, we measured the RNAP concentration to be 17% lower than in

329   1X (Fig. 5A) and no morphological changes. Thus, we assume the free RNAP in 0.5X to equal ~120/cell.

330   Next, we fitted the equations (8) and (9) relating d_{TSS} with $\log_{10}$ (M_P) in all interference models (Table 1),

331   using the data on M_P in 1X medium (Fig 6A) and the 'fit' function of MATLAB. For this, we set $k^{\max} = k_{occupy}^{\max}$

332    $= k_{ocl}^{\max}$, for simplicity, as well as realistic bounds for each parameter to infer. To avoid local minima, we

333   performed 200 searches, each starting from a random initial point, and selected the one that maximized

334   R^2. Results are shown in Table 3.

335   Next, we inserted all parameter values (empirical and inferred) in Equations (10) and (11) to predict CV_P^2

336   and S_P in 1X medium (Figs 6B and 6C). Also, we inserted the same parameter values and the estimated

337   RNAP numbers in 0.5X medium in equations (8-11) to obtain the analytical solutions for M_P, CV_P^2 and S_P

338   for 0.5X medium (Figs 6D, 6E and 6F).

339   From Fig. 6, the data is 'noisy', which suggests that it is not possible to establish if the models are

340   significantly different. As such, here we only select the one that best explains the data, based on the R^2

341   values of the fittings. Table 3 shows the mean R^2 for M_P, CV_P^2, and S_P when confronting the model with

342   the data. Overall, from the R^2 values, the step model is the one that best fits the data. Meanwhile, the

343   'ZeroO' model is the least accurate, which supports the existence of distinct kinetics when d_{TSS} is smaller

344   or larger than 35 nucleotides, which is the length of the RNAP when committed to OC on the TSS [23-25].

345   In summary, the proposed model of expression of genes under the control of a pair of tandem promoters is

346   based on a standard model of transcription of each promoter, which are subject to interference, either due

347   to occlusion of the TSSs or by RNAP occupying the downstream promoter on the TSS of the downstream

348   promoter. The influence of each occurrence of these events is well modeled by linear functions of TSS

349   occupancy times, while their dependency on d_{TSS} is modeled by a continuous step function. If d_{TSS} is larger

350   than 35 bp, effects from the RNAP occupying the downstream promoter can occur, else occlusion can
351   occur.

352   **Table 2. Parameter values imposed identically on all models.**

Parameter description	Parameter	Value	References
Inverse of the mean time to complete OC	k_{after}	0.005 s^{-1}	Differs between promoters. Since empirical data lacks, we used the data from *in vivo* single RNA measures for Lac-Ara-1 [20].
RNA and protein dilution due to division	$k_{dil} = \dfrac{\ln(2)}{D}$	1.005×10^{-4} s^{-1}	Legend of Fig S8
RNA degradation	k_{rdeg}	2.3×10^{-3} s^{-1}	[28]
RNA decay due to dilution from cell division and due to degradation	$k_{rd} = k_{rdeg} + k_{dil}$	2.4×10^{-3} s^{-1}	From row 2.
Protein degradation	k_{pdeg}	2.93×10^{-5} s^{-1}	[47], estimates it to be from ~6×10^{-5} to ~2×10^{-5}. We used the value in [48], in that interval.
Protein decay due to dilution by cell division and degradation	$k_{pd} = k_{pdeg} + k_{dil}$	1.3×10^{-4} s^{-1}	From rows 2 and 5.
Fall-off probability of the RNAP occupying the downstream promoter	f	50% (0.5)	Set here (likely sequence-dependent)
Protein production rate constant	$k_p = C_1 \times (k_{pd} + k_{rd})$	0.18 s^{-1}	C_1 is estimated here.
Free RNAP per cell	$[R]$	144/cell in 1X and 120/cell in 0.5X media	See main text.

353

354   **Table 3. Parameter values inferred for each model**.

Interference model	Inferred parameter values	Average R^2 (M, CV^2, S) 1X medium	Average R^2 (M, CV^2, S) 0.5X medium
Exponential 1	$k_{bind} \cdot [R] = 1.09 \times 10^{-2}$ s^{-1} × (cell vol)$^{-1}$ $k_{bind} = 7.53 \times 10^{-5}$ s^{-1}	0.21 (Figs. 6A, 6B, and 6C)	0.09 (Figs. 6D, 6E, and 6F)

|			
	k_{unbind} = 0.84 s^{-1} k^{max} = 677.7 s^{-1} b_1 = 5.08 × 10^{-2} bp^{-1}		
Exponential 2	$k_{bind} \cdot [R]$ = 9.71 × 10^{-3} s^{-1} × (cell vol)$^{-1}$ k_{bind} = 6.74 × 10^{-5} s^{-1} k_{unbind} = 0.80 s^{-1} k^{max} = 554.8 s^{-1} b_1 = 7.92 × 10^{-8} bp^{-1} b_2 = 1.47 × 10^{-3} bp^{-2}	0.25 (Figs. 6A, 6B, and 6C)	0.12 (Figs. 6D, 6E, and 6F)
Step	$k_{bind} \cdot [R]$ = 6.62 × 10^{-3} s^{-1} × (cell vol)$^{-1}$ k_{bind} = 4.60 × 10^{-5} s^{-1} k_{unbind} = 0.49 s^{-1} k^{max} = 313.4 s^{-1} L = 35.11 bp (by best fitting, which corresponds to 35 bp)	0.35 (Figs. 6A, 6B, and 6C)	0.15 (Figs. 6D, 6E, and 6F)
zero order	$k_{bind} \cdot [R]$ = 4.63 × 10^{-3} s^{-1} × (cell vol)$^{-1}$ k_{bind} = 3.22 × 10^{-5} s^{-1} k_{unbind} = 0.57 s^{-1} k^{max} = 6.48 s^{-1}	-0.007 (Figs. 6A, 6B, and 6C)	-0.12 (Figs. 6D, 6E, and 6F)

355
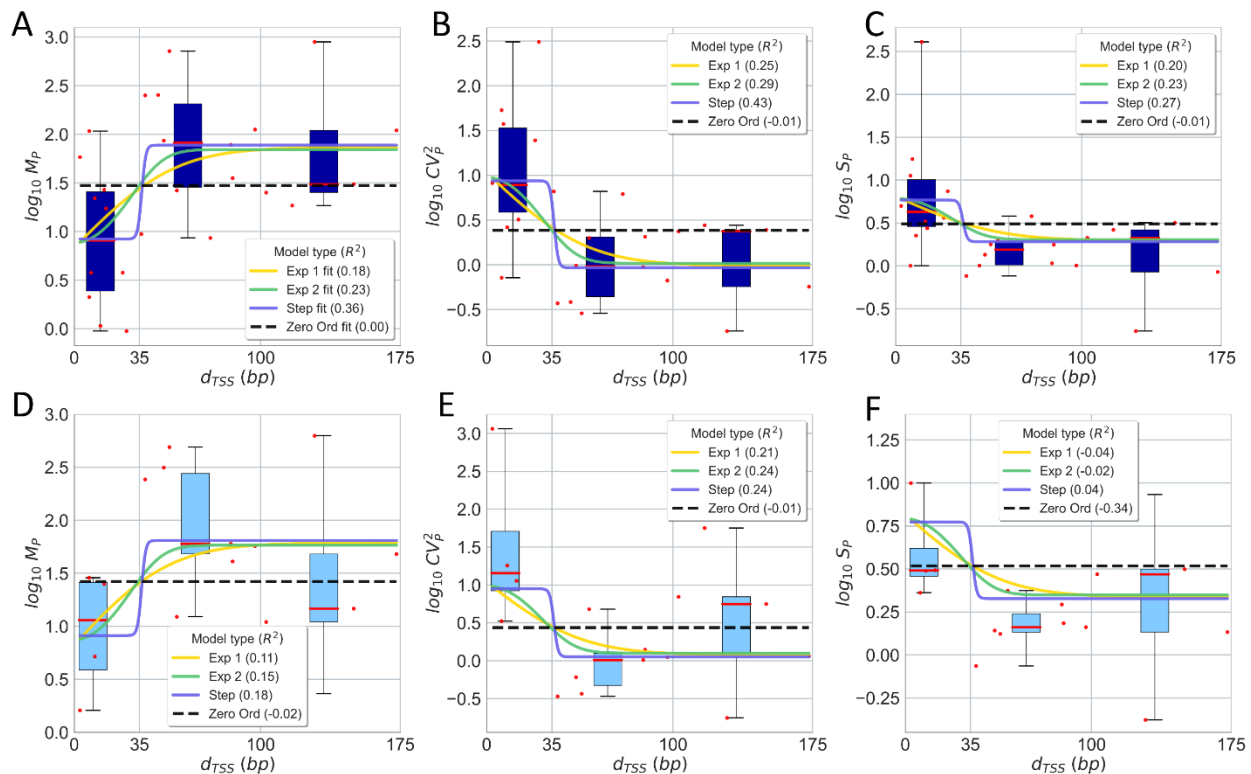
Fig 6. **Empirical data and analytical model of how d_{TSS} influences the single-cell protein numbers of genes controlled by tandem promoters. (A)** Mean, **(B)** CV^2, and **(C)** S of single protein numbers in the **1X** media as a function of d_{TSS}. **(D)**, **(E),** and **(F)** show the same for the **0.5X** media, respectively. Each red dot is the mean from 3 biological repeats for a pair of promoters (S6 Table). The dots were also grouped in 3 'boxes' based on their d_{TSS}. In each box, the red line is the median and the top and bottom are the 3rd and 1st quartiles, respectively. The vertical black bars are the range between minimum and maximum of the red dots. In **A**, all lines are best fits. In **B**, **C**, **D**, **E**, and **F**, all lines are model predictions, based on the parameters used to best fit **A**. The insets show the R^2 for each model fit and prediction.

We then confronted the analytical solutions of the step model with stochastic simulations (Section 'Stochastic simulations for the step inference model' in the S1 Appendix). We first assumed various d_{TSS}, but fixed k_{bind} , for simplicity. Visibly, M_P, CV_P^2 , and S_P of the stochastic simulations are well-fitted by the analytical solution, supporting the initial assumption that CV_P^2 , and S_P follow a negative binomial (Fig S13 in the S2 Appendix).

However, natural promoters are expected to differ in k_{bind} as they differ in sequence [49-50]. Thus, we introduced this variability and studied whether the analytical model holds. To change the variability, we

18

374   obtained each k_{bind} from gamma distributions (means shown in Table 3 and CVs in Table S9 in the S3

375   Appendix). We chose a gamma distribution since its values are non-negative and non-integer (such as rate

376   constants). Meanwhile, all parameters of the step model, aside from k_{bind}, are obtained from Tables 2 and

377   3. For $d_{TSS} \leq 35$ and $d_{TSS} > 35$, and each CV considered, we sampled 10.000 pairs of values of $k_{bind} \cdot [R]$,

378   and calculated M, CV² and S for each of them. Next, we estimated the average and standard deviation of

379   each statistics. From Fig S14 in the S2 Appendix, if $CV(k_{bind}) < 1$, the analytical solution is robust. In

380   that the standard error of the mean is smaller than $M_P/3$. Notably, for such CV, the strength of the two paired

381   promoters would have to differ unrealistically by more than 2000%, on average (Table S9 in the S3

382   Appendix). Thus, we find the analytical solution to be reliable.

383   From our estimation of k_p, we further estimated a protein-to-RNA ratio, $\dfrac{M_P}{M_{RNA}} = \dfrac{k_p}{k_{pd}}$. From Eq. 8 and

384   Table 2, we find that $\dfrac{k_p}{k_{pd}}$ ~ 1418 in both media, which agrees with previous estimations (~1832 in 27]).

385

386   Next, we used the fitted model to predict (using Eqs. 8 to 11) the influence of promoter occupancy (ω) on

387   the M_P, CV_P^2 and S_P of upstream and downstream promoters. We set d$_{TSS}$ to 20 bp to represent

388   promoters where ≤ 35, and to 100 bp to represent promoters with $d_{TSS} > 35$. Then, for each cohort, we

389   changed ω from 0.01 to 0.99 (i.e., nearly all possible values). In addition, we estimated these moments

390   when $k_{occlusion}$, k_{occupy}, and ω are all set to zero (i.e., the two promoters do not interfere), for comparison.

391   From Fig. 7, a pair of tandem promoters can produce less proteins than a single promoter with the same

392   parameter values, if $d_{TSS} \leq 35$, which makes occlusion possible. Meanwhile, if $d_{TSS} > 35$, tandem promoters

393   can only produce protein numbers in between the numbers produced by one isolated promoter and the

394   numbers produced by two isolated promoters. In no case can two interfering tandem promoters produce

395   more than two isolated promoters with equivalent parameter values. I.e., according to the model, the

396   interference between tandem promoters cannot enhance production.

397   Meanwhile, the kinetics of the upstream (Figs. 7A and S15A in the S2 Appendix) and downstream

398   promoters (Figs. 7B and S15B in the S2 Appendix) only differ in that the downstream promoter is more

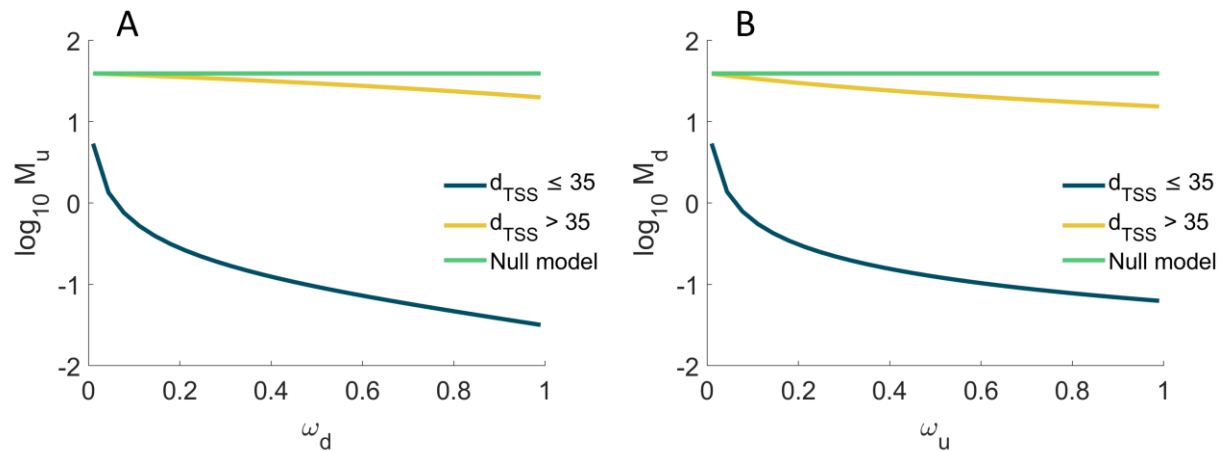399   responsive to ω.

400

Fig 7. Mean protein numbers produced as a function of other promoter's occupancy. M_P of the single-cell distribution of the number of proteins produced (**A**) by the upstream promoter alone, and (**B**) by the downstream promoter alone. Results are shown as a function of the fraction of times that the upstream (0.01 ≤ ω_u ≤ 0.99) and the downstream (0.01 ≤ ω_d ≤ 0.99) promoter are occupied by RNAP. The null model is estimated by setting $k_{occlusion}$, k_{occupy}, and ω to zero.

Finally, consider that the model predicts that transcription interference should occur in tandem promoters, either due to occlusion if $d_{TSS} \leqslant 35$ occupancy or due to occupancy of the downstream promoter if d_{TSS} > 35. Meanwhile, in single promoters, neither of these phenomena occurs. Thus, on average, two single promoters should produce more RNA and proteins than a pair of tandem promoters of similar strength. Using the genome wide data from [28] on protein expression levels during exponential growth we estimated the double of the mean expression level (it equals 183.8) of genes controlled by single promoters (section 'Selection of natural genes controlled by single promoters' in the S1 Appendix). Meanwhile, also using data from [28], the mean expression level of genes controlled by tandem promoters equals 148 (estimated from the 26 that they have reported on), in agreement with the hypothesis. Nevertheless, this data is subject to external variables (e.g., TF interference). A definitive test would require the use of synthetic constructs, lesser affected by external influences.

Regulatory parameters of promoter occupancy and occlusion

Since the occupancy, ω, of each of the tandem promoters is responsible for transcriptional interference by occlusion and by RNAPs occupying the downstream promoter, we next explored the biophysical limits of ω. Eqs. 6a and 6b define the occupancies of the upstream and downstream promoters, ω_u and ω_d,

20

422   respectively. For simplicity, here we refer to both of them as ω . Fig. 8A shows that ω increases with the

423   rate of RNAP binding ($k_{bind} \cdot [R]$), but only within a certain range of (high) values of the time from binding

424   to elongating (k_{after}^{-1}). I.e., RNAPs need to spend a significant time in OC, if they are to cause interference,

425   which is expected. Similarly, ω changes with k_{after}^{-1}, but only for high values of $k_{bind} \cdot [R]$. I.e., if it's rare

426   for RNAPs to bind, the occupancy will necessarily be weak.

427   In detail, from Fig. 8A, ω can change significantly within $10^{-2} < k_{bind} \times [R] < 10$ s^{-1} and $10^{-2} < k_{after}^{-1} < 10^2$ s^{-1}.

428   For these ranges, we expect RNA production rates (k_r, equations 5a, 5b, 6b, 7 and 9) to vary from ~10^{-5} (if

429    $d_{TSS} \leq 35$) and ~10^{-4} (if $d_{TSS} > 35$) until 10 s^{-1}. In agreement, in *E. coli*, promoters have RNA production rates

430   from ~10^{-3} to 10^{-1} s^{-1} when induced [20-21, 39, 51-52]and ~10^{-4} to 10^{-6} s^{-1} when non-fully active [28]. Thus,

431   ω can differ within realistic intervals of parameter values.

432   Next, we estimated $k_{occlusion}$, the rate at which a promoter occludes the other as a function of d_{TSS} and ω

433   using Equations 6a and 6b. k^{max} is shown in Table 3. To model $I(d_{TSS})$ we used the step function in Table

434   1. Overall, $k_{occlusion}$ changes linearly with ω , when and only when $d_{TSS} \leq 35$ (Fig. 8B).
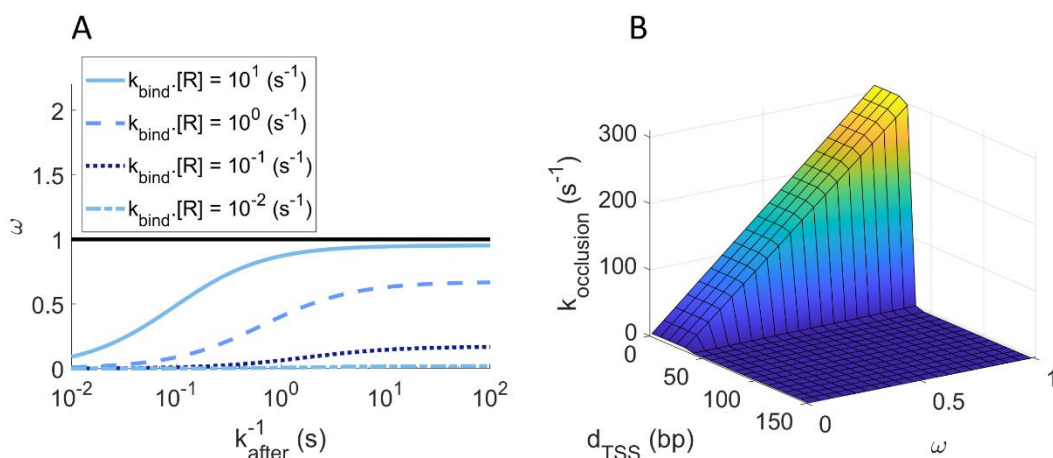

435

436   **Fig 8. Promoter occupancy ω estimated for the step model.** (A) ω as a function of the rate constant

437   for a *free* RNAP to bind to the *unoccupied* promoter ($k_{bind} \cdot [R]$) and of the time for that RNAP to start

438   elongation after commitment to OC, k_{after}^{-1}. The horizontal black line at $\omega = 1$, is the maximum fraction of

439   time that the promoter can be occupied (i.e., the maximum promoter occupancy). (B) $k_{occlusion}$ plotted as a

21

440   function of ω and d_{TSS}. Since $k_{occlusion}$ increases with ω if and only if $d_{TSS} \leq 35$, it renders the simultaneous

441   occupation of both TSS's impossible.

442

State space of the single cell statistics of protein numbers of tandem promoters

445   We next studied how much the single-cell statistics of protein numbers (M_P, CV_P^2, and S_P) of the upstream,

446   'u', and downstream, 'd', promoters changes with ω_u, ω_d, and d_{TSS}. Here, ω_u and ω_d are increased from

447   0 to 1 by increasing the respective k_{bind} (Eqs. 6a and 6b).

448   From Fig. 9A, if $d_{TSS} \leq 35$ bp, reducing ω_d while also increasing ω_u is the most effective way to increase

449   M_u, since this increases the number of RNAPs transcribing from the upstream promoter that are not

450   hindered by RNAPs occupying the downstream promoter. If $d_{TSS} > 35$ bp, the occupancy the downstream

451   promoter, ω_d, becomes ineffective.

452   Oppositely, from Fig. 9B, if $d_{TSS} \leq 35$ bp, increasing ω_d while also decreasing ω_u, is the most effective way

453   to increase M_d since this increases the number of RNAPs transcribing from the downstream promoter does

454   not interfere by RNAPs elongating from the upstream promoter. If $d_{TSS} > 35$ bp, the occupancy the upstream

455   promoter, ω_u, becomes ineffective.

456   Finally, from Fig. 9C, regardless of d_{TSS}, for small ω_d and ω_u, as the occupancies increase, M_t increases

457   quickly and in a non-linear fashion. However, as both ω_d and ω_u reach high values, M_t decreases for

458   further increases, if $d_{TSS} \leq 35$ bp. Instead, if $d_{TSS} > 35$ bp, M_t appears to saturate.

459   From Figs. S16 in the S2 Appendix, CV_P^2 and S_P behave inversely to M_P.

460   Relevantly, in all cases, the range of predicted protein numbers (Fig. 9C1) are in line with the empirical

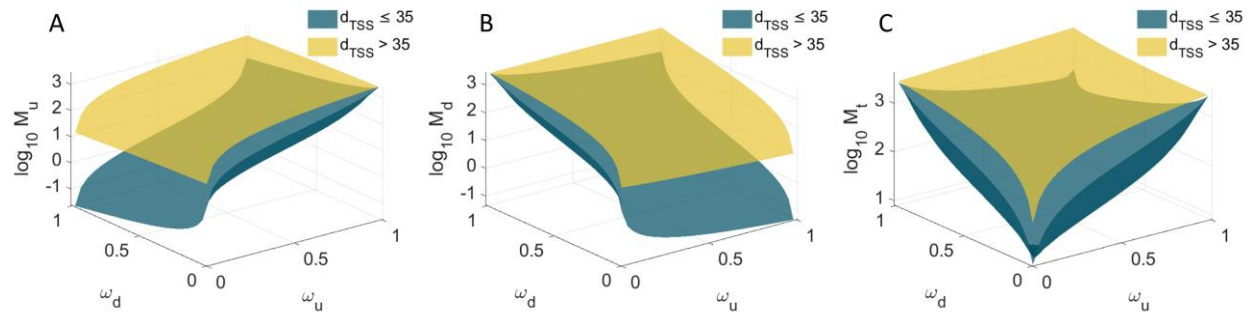461   values (~10^{-1} to 10^3 proteins per cell) (Fig. 4D).

462

Fig 9. Mean protein expression as a function of both promoters' occupancy. Expected mean protein numbers due to the activity of: (**A**) the upstream promoter alone, (**B**) the downstream promoter alone, and (**C**) both promoters. M_P is shown as a function of the fraction of times that the upstream ($0 \leq \omega_u \leq 1$) and the downstream ($0 \leq \omega_d \leq 1$) promoters are occupied by RNAP, when $d_{TSS} > 35$ (yellow) and $d_{TSS} \leq 35$ (dark green) bp.

Discussion

E. coli genes controlled by tandem promoters have a relatively high mean conservation level (0.2, while the average gene has 0.15, with a p-value of 0.009), suggesting that they play particularly relevant biological roles (section 'Gene Conservation' in the S1 Appendix). From empirical data on single-cell protein numbers of 30 *E. coli* genes controlled by tandem promoters, we found evidence that their dynamics is subject to RNAP interference between the two promoters. This interference reduces the mean single-cell protein numbers, while increasing its CV^2 and skewness, and can be tuned by ω, the promoters' occupancy by RNAP, and by d_{TSS}. Since both of these parameters are sequence dependent [21, 31] the interference should be evolvable. Further, since ω of at least some of these genes should be under the influence of their several input TFs, the interference has the potential to be adaptive.

We proposed models of the dynamics of these genes as a function of ω and d_{TSS}, using empirically validated parameter values. In our best fitting model, transcription interference is modelled by a step function of d_{TSS} (instead of gradually changing with d_{TSS}), since the only detectable differences in dynamics with changing d_{TSS} were between tandem promoters with $d_{TSS} \leq 35$ and $d_{TSS} > 35$ nucleotides (the latter cohort of genes having higher mean expression and lower variability). We expect that causes this difference tangible is the existence of the OC formation. In detail, the OC is a long-lasting DNA-RNAP formation that occupies that strict region of DNA at the promoter region [24, 31]. As such, occlusion should share these physical features. Because of that, when $d_{TSS} \leq 35$, an RNAP bound to TSS always occludes the other TSS, significantly reducing RNA production. Meanwhile, if $d_{TSS} > 35$, interference occurs when an RNAP elongating from the upstream promoter is obstructed by an RNAP occupying the downstream promoter.

23

488   Meanwhile, contrary to d_{TSS}, if one considers realistic ranges of the other model parameters, it is possible
489   to predict a very broad range of accessible dynamics for tandem promoter arrangements. This could explain
490   the observed diversity of single-cell protein numbers as a function of d_{TSS} (Fig 6). At the evolutionary level,
491   such potentially high range of dynamics may provide high evolutionary adaptability and thus, it may be one
492   reason why genes controlled by these promoters are relatively more conserved.

493   One potentially confounding effect which was not accounted for in this model is the accumulation of
494   supercoiling. Closely spaced promoters may be more sensitive to supercoiling buildup than single
495   promoters [53-55]. If so, it will be useful to extend the model to include these effects [26]. Using such model
496   and measurements of expression by tandem promoters when subject to, e.g. Novobiocin [56], may be of
497   use to infer kinetic parameters of promoter locking due to positive supercoiling build-up.

498   Other potential improvements could be expanding the model to tandem arrangements other than I and II
499   (Fig 1), to include a third form of interference (transcription elongation of a nearby gene).

500   One open question is whether placing promoters in tandem formation increases the robustness of
501   downstream gene expression to perturbations (e.g., fluctuations in the concentrations of RNAP or TF
502   regulators). A tandem arrangement likely increases the robustness to perturbations which only influence
503   one of the promoters. Another open question is why several of the 102 tandem promoters with
504   arrangements I and II appeared to behave independently from their input TFs (according to the RNA-seq
505   data), albeit having more input TFs (1.62 on average) than expected by chance (the average *E. coli* gene
506   only has 0.95). As noted above, we hypothesize that these input TFs may become influential in conditions
507   other than the ones studied here.

508   Here, we also did not consider any influence from the phenomenon of "RNAP cooperation" [57]. This is
509   based on this being an occurrence in elongation, and we expect interactions between two *elongating*
510   RNAPs to rarely affect the interference between tandem promoters [9]. However, potentially, it could be of
511   relevance in the strongest tandem promoters.

512   Finally, a valuable future study on tandem promoters will require the use of synthetic tandem promoters
513   (integrated in a specific chromosome location) that systematically differ in promoter strengths and
514   nucleotide distances. This would allow extracting parameter values associated to promoter interference to
515   create a more precise model than the one based on the natural promoters (which is influenced by TFs, etc).
516   Similarly, measuring the strength of individual natural promoters would contribute to this effort.

517   Overall, our model, based on a significant number of natural tandem promoters whose genes have a wide
518   range of expression levels, should be applicable to the natural tandem promoters not observed here (at
519   least of arrangements I and II), including of other bacteria, and to be accurate in predicting the dynamics of
520   synthetic promoters in these arrangements.

24

521 Currently, predicting how gene expression kinetics change with the promoter sequence remains
522 challenging. Even single- or double-point mutants of known promoters behave unpredictably, likely because
523 the individual sequence elements influence the OC and CC in a combinatorial fashion. Consequently, the
524 present design of synthetic circuits is usually limited to the use of a few promoters whose dynamics have
525 been extensively characterized (Lac, Tet, etc.). This severely limits present synthetic engineering.

526 We suggest that a promising methodology to create new synthetic genes with a wide range of predictable
527 dynamics is to assemble well-characterized promoters in a tandem formation, and to tune their target
528 dynamics using our model. Specifically, for a given dynamics, it is possible to invert the model and find a
529 suitable pair of promoters with known occupancies and corresponding d_{TSS} (smaller or larger than 35),
530 which achieve these dynamics. A similar strategy was recently proposed in order to achieve strong
531 expression levels [58]. Our results agree and further expand on this by showing that the mean expression
532 level can also be reduced and expression variability can further be fine-tuned.

533 Importantly, this can already be executed, e.g., using a library of individual genes whose expression can
534 be measured [28]. From this library, we can select any two promoters of interest and arrange them as
535 presented here, in order to obtain a kinetics of expression as close as possible to a given target. Note that
536 these dynamics have a wide range, from weaker to stronger than that of either promoter (albeit no stronger
537 than their sum, Fig 9C1-C3). Given the number of natural genes whose expression is already known and
538 given the present accuracy in assembling specific nucleotide sequences, we expect this method to allow
539 the rapid engineering of genes with desired dynamics with an enormous range of possible behaviours. As
540 such, these constructs could represent a recipe book for the components of gene circuits with predictable
541 complex kinetics.

Materials and Methods

543 Using information from RegulonDB v10.5 as of 30th of January 2020, we started by searching natural genes
544 controlled by two promoters (Section 'Selection of natural genes controlled by tandem promoters' in the S1
545 Appendix). Next, we studied their evolutionary conservation and ontology (Sections 'Gene conservation'
546 and 'Gene Ontology' in the S1 Appendix) and analysed their local topological features within the TFN of *E.*
547 *coli* (Section 'Network topological properties' in the S1 Appendix).

548 RNA-seq measurements were conducted in two points in time (Section 'RNA-seq measurements and data
549 analysis' in the S1 Appendix), to obtain fold changes in RNA numbers of genes controlled by tandem
550 promoters with arrangements I and II, their input TFs, and their output genes (Fig 1). We used this data to
551 search for relationships between input and output genes.

552 Next, a model of gene expression was proposed, and reduced to obtain an analytical solution of the single-
553 cell protein expression statistics of tandem promoters (Sections 'Derivation of mean protein expression of

554 the model' and 'Derivation of CV^2 and skewness of protein expression of the model' in the S1 Appendix).

555 This analytical solution was compared to stochastic simulations conducted using the simulator SGNS2.

556 (Section 'Stochastic simulations for the step inference model' in the S1 Appendix).

557 We collected single-cell flow-cytometry measurements of 30 natural genes controlled by tandem promoters

558 (Section 'Flow-cytometry and data analysis' in the S1 Appendix) to validate the model. For this, first, from

559 the original data, we subtracted the cellular background fluorescence (Section 'Subtraction of background

560 fluorescence from the total protein fluorescence' in the S1 Appendix). Then, we converted the fluorescence

561 intensity into protein numbers (Section 'Conversion of protein fluorescence to protein numbers in the S1

562 Appendix). From this we obtained empirical data on $M, CV^2, and S$ of the single-cell distributions of protein

563 numbers in two media (Sections 'Media and chemicals' and 'Strains and growth conditions' in the S1

564 Appendix). Flow-cytometry measurements were also compared to microscopy data, supported by image

565 analysis (Section 'Microscopy and Image analysis' in the S1 Appendix), for validation.

566 Comparing the data from RegulonDB (30.01.2020) used here, with the most recent (21.07.2021), we found

567 that the numbers of genes controlled by tandem promoters of arrangements I and II differed by ~4% (from

568 102 to 98). Regarding those whose activity was measured by flow-cytometry, this difference is ~3% (30 to

569 31). Globally, 163 TF-gene interactions differed (~3.4%) while for the 98 genes controlled by tandem

570 promoters of arrangements I and II, only 10 TF-gene interactions differ (~2.7%). Finally, globally the

571 numbers of TUs differed by ~1%, promoters by ~0.6%, genes by ~1%, and terminators by ~15% (which did

572 not affect the genes studied, as they changed by ~4% only). These small differences should not affect our

573 conclusions.

574 Finally, a data package [59] is provided in Dryad with flow-cytometry and microscopy data and codes used.

Supporting Information

575

576 **S1 Appendix. Extended Methods and Materials.** (PDF)

577 **S2 Appendix. Supporting Figures**. (PDF)

578 **S3 Appendix. Supporting Tables**. (PDF)

579 **S4 Appendix. Supporting Results**. (PDF)

580 **S5 Table. Gene Ontology**. Overrepresentation tests using the PANTHER Classification System. List of

581 biological processes which are overrepresented using Fisher's exact tests are shown. (Excel)

582 **S6 Table. Protein statistics**. Statistics of single-cell distributions of protein fluorescence of genes

583 controlled by tandem promoters as measured by flow-cytometry in 1X and 0.5X diluted M9 media

584 conditions. (Excel)

585 **S7 Table. Protein statistics**. Statistics of single-cell distributions of protein fluorescence of genes
586 controlled by single promoter as measured by flow-cytometry in 1X M9 media condition. (Excel)

Acknowledgements

References

591 1. Herbert M, Kolb A, Buc H. Overlapping promoters and their control in Escherichia coli: the gal case.
592   Proc Natl Acad Sci U S A. 1986;83: 2807–2811. doi:10.1073/pnas.83.9.2807
593

594 2. Beck CF, Warren RA. Divergent promoters, a common form of gene organization. Microbiol Rev.
595   1988;52: 318–326. doi:10.1128/mr.52.3.318-326.1988
596

597 3. Adachi N, Lieber MR. Bidirectional gene organization: a common architectural feature of the human
598   genome. Cell. 2002;109: 807–809. doi:10.1016/s0092-8674(02)00758-4
599

600 4. Trinklein ND, Aldred SF, Hartman SJ, Schroeder DI, Otillar RP, Myers RM. An abundance of
601   bidirectional promoters in the human genome. Genome Res. 2004;14: 62–66.
602   doi:10.1101/gr.1982804
603

604 5. Shearwin KE, Callen BP, Egan JB. Transcriptional interference--a crash course. Trends Genet.
605   2005;21: 339–345. doi:10.1016/j.tig.2005.04.009
606

607 6. Prescott EM, Proudfoot NJ. Transcriptional collision between convergent genes in budding yeast.
608   Proc Natl Acad Sci U S A. 2002;99: 8796–8801. doi:10.1073/pnas.132270899
609

610 7. Korbel JO, Jensen LJ, von Mering C, Bork P. Analysis of genomic context: prediction of functional
611   associations from conserved bidirectionally transcribed gene pairs. Nat Biotechnol. 2004;22: 911–
612   917. doi:10.1038/nbt988
613

614 8. Wei W, Xiang H, Tan H. Two tandem promoters to increase gene expression in Lactococcus lactis.
615   Biotechnol Lett. 2002;24: 1669–1672. doi:10.1023/A:1020653417455
616

617 9. Sneppen K, Dodd IB, Shearwin KE, Palmer AC, Schubert RA, Callen BP, et al. A mathematical
618   model for transcriptional interference by RNA polymerase traffic in Escherichia coli. J Mol Biol.
619   2005;346: 399–409. doi: 10.1016/j.jmb.2004.11.075
620

621 10. Martins L, Mäkelä J, Häkkinen A, Kandhavelu M, Yli-Harja O, Fonseca JM, et al. Dynamics of
622   transcription of closely spaced promoters in Escherichia coli, one event at a time. J Theor Biol.
623   2012;301: 83–94. doi:10.1016/j.jtbi.2012.02.015
624

625 11. Horowitz H, Platt T. Regulation of transcription from tandem and convergent promoters. Nucleic
626   Acids Res. 1982;10: 5447–5465. doi:10.1093/nar/10.18.5447
627

12. Bordoy AE, Varanasi US, Courtney CM, Chatterjee A. Transcriptional Interference in Convergent Promoters as a Means for Tunable Gene Expression. ACS Synth Biol. 2016;5: 1331–1341. doi:10.1021/acssynbio.5b00223

13. Palmer AC, Ahlgren-Berg A, Egan JB, Dodd IB, Shearwin KE. Potent transcriptional interference by pausing of RNA polymerases over a downstream promoter. Mol Cell. 2009;34: 545–555. doi:10.1016/j.molcel.2009.04.018

14. Callen BP, Shearwin KE, Egan JB. Transcriptional Interference between Convergent Promoters Caused by Elongation over the Promoter. Mol Cell. 2004;14: 647–656. doi:10.1016/j.molcel.2004.05.010

15. Hoffmann SA, Hao N, Shearwin KE, Arndt KM. Characterizing Transcriptional Interference between Converging Genes in Bacteria. ACS Synth Biol. 2019;8: 466–473. doi:10.1021/acssynbio.8b00477

16. Masulis IS, Babaeva ZS, Chernyshov SV, Ozoline ON. Visualizing the activity of Escherichia coli divergent promoters and probing their dependence on superhelical density using dual-colour fluorescent reporter vector. Sci Rep. 2015;5: 1–10. doi:10.1038/srep11449

17. Vogl T, Kickenweiz T, Pitzer J, Sturmberger L, Weninger A, Biggs BW, et al. Engineered bidirectional promoters enable rapid multi-gene co-expression optimization. Nat Commun. 2018;9: 1–13. doi:10.1038/s41467-018-05915-w

18. Adhya S, Gottesman M. Promoter occlusion: Transcription through a promoter may inhibit its activity. Cell. 1982;29: 939–944. doi:10.1016/0092-8674(82)90456-1

19. Eszterhas SK, Bouhassira EE, Martin DIK, Fiering S. Transcriptional interference by independently regulated genes occurs in any relative arrangement of the genes and is influenced by chromosomal integration position. Mol Cell Biol. 2002;22: 469–479. doi:10.1128/MCB.22.2.469-479.2002

20. Lloyd-Price J, Startceva S, Kandavalli V, Chandraseelan JG, Goncalves N, Oliveira SMD, et al. Dissecting the stochastic transcription initiation process in live Escherichia coli. DNA Res. 2016;23: 203–214. doi:10.1093/dnares/dsw009

21. Lutz R, Lozinski T, Ellinger T, Bujard H. Dissecting the functional program of Escherichia coli promoters: the combined mode of action of Lac repressor and AraC activator. Nucleic Acids Res. 2001;29: 3873–3881. doi:10.1093/nar/29.18.3873

22. McClure WR. Rate-limiting steps in RNA chain initiation. Proc Natl Acad Sci U S A. 1980;77: 5634–5638. doi:10.1073/pnas.77.10.5634

23. Krummel B, Chamberlin MJ. Structural analysis of ternary complexes of Escherichia coli RNA polymerase. Deoxyribonuclease I footprinting of defined complexes. J Mol Biol. 1992;225: 239–250. doi:10.1016/0022-2836(92)90918-a

24. deHaseth Pieter L., Zupancic Margaret L., Record M. Thomas. RNA Polymerase-Promoter Interactions: the Comings and Goings of RNA Polymerase. J Bacteriol. 1998;180: 3019–3025. doi:10.1128/JB.180.12.3019-3025.1998

25. Greive SJ, von Hippel PH. Thinking quantitatively about transcriptional regulation. Nat Rev Mol Cell Biol. 2005;6: 221–232. doi:10.1038/nrm1588

26. Palma CSD, Kandavalli V, Bahrudeen MNM, Minoia M, Chauhan V, Dash S, et al. Dissecting the in vivo dynamics of transcription locking due to positive supercoiling buildup. Biochimica et Biophysica Acta (BBA) - Gene Regulatory Mechanisms. 2020;1863: 194515. doi: 10.1016/j.bbagrm.2020.194515

27. Häkkinen A, Oliveira SMD, Neeli-Venkata R, Ribeiro AS. Transcription closed and open complex formation coordinate expression of genes with a shared promoter region. J R Soc Interface. 2019;16: 20190507. doi:10.1098/rsif.2019.0507

28. Taniguchi Y, Choi PJ, Li G-W, Chen H, Babu M, Hearn J, et al. Quantifying E. coli Proteome and Transcriptome with Single-Molecule Sensitivity in Single Cells. Science. 2010;329: 533–538. doi:10.1126/science.1188308

29. Friedman LJ, Mumm JP, Gelles J. RNA polymerase approaches its promoter without long-range sliding along DNA. Proc Natl Acad Sci U S A. 2013;110: 9740–9745. doi:10.1073/pnas.1300221110

30. Skinner GM, Baumann CG, Quinn DM, Molloy JE, Hoggett JG. Promoter Binding, Initiation, and Elongation by Bacteriophage T7 RNA Polymerase: A SINGLE-MOLECULE VIEW OF THE TRANSCRIPTION CYCLE*. J Biol Chem. 2004;279: 3239–3244. doi:10.1074/jbc.M310471200

31. McClure WR. Mechanism and control of transcription initiation in prokaryotes. Annu Rev Biochem. 1985;54: 171–204. doi:10.1146/annurev.bi.54.070185.001131

32. Saecker RM, Record MT Jr, Dehaseth PL. Mechanism of bacterial transcription initiation: RNA polymerase - promoter binding, isomerization to initiation-competent open complexes, and initiation of RNA synthesis. J Mol Biol. 2011;412: 754–771. doi:10.1016/j.jmb.2011.01.018

33. Mekler V, Kortkhonjia E, Mukhopadhyay J, Knight J, Revyakin A, Kapanidis AN, et al. Structural Organization of Bacterial RNA Polymerase Holoenzyme and the RNA Polymerase-Promoter Open Complex. Cell. 2002;108: 599–614. doi:10.1016/S0092-8674(02)00667-0

34. Margeat E, Kapanidis AN, Tinnefeld P, Wang Y, Mukhopadhyay J, Ebright RH, et al. Direct Observation of Abortive Initiation and Promoter Escape within Single Immobilized Transcription Complexes. Biophys J. 2006;90: 1419–1431. doi:10.1529/biophysj.105.069252

35. Hsu LM. Promoter clearance and escape in prokaryotes. Biochim Biophys Acta. 2002;1577: 191–207. doi:10.1016/s0167-4781(02)00452-9

36. Hsu LM. Promoter Escape by Escherichia coli RNA Polymerase. EcoSal Plus. 2008;3. doi:10.1128/ecosalplus.4.5.2.2

37. Henderson KL, Felth LC, Molzahn CM, Shkel I, Wang S, Chhabra M, et al. Mechanism of transcription initiation and promoter escape by E. coli RNA polymerase. Proc Natl Acad Sci U S A. 2017;114: E3032–E3040. doi:10.1073/pnas.1618675114

38. Ponnambalam S, Busby S. RNA polymerase molecules initiating transcription at tandem promoters can collide and cause premature transcription termination. FEBS Lett. 1987;212: 21–27. doi:10.1016/0014-5793(87)81549-1

39. Kandavalli VK, Tran H, Ribeiro AS. Effects of σ factor competition are promoter initiation kinetics dependent. Biochim Biophys Acta. 2016;1859: 1281–1288. doi: 10.1016/j.bbagrm.2016.07.011

731

732   40. Bremer H, Dennis P, Ehrenberg M. Free RNA polymerase and modeling global transcription in
733   Escherichia coli. Biochimie. 2003;85: 597–609. doi:10.1016/S0300-9084(03)00105-6

734

735   41. Patrick M, Dennis PP, Ehrenberg M, Bremer H. Free RNA polymerase in Escherichia coli.
736   Biochimie. 2015;119: 80–91. doi:10.1016/j.biochi.2015.10.015

737

738   42. Ju X, Li D, Liu S. Full-length RNA profiling reveals pervasive bidirectional transcription terminators
739   in bacteria. Nat Microbiol. 2019;4: 1907–1918. doi:10.1038/s41564-019-0500-z

740

741

742   43. Santos-Zavaleta A, Salgado H, Gama-Castro S, Sánchez-Pérez M, Gómez-Romero L, Ledezma-
743   Tejeida D, et al. RegulonDB v 10.5: tackling challenges to unify classic and high throughput
744   knowledge of gene regulation in E. coli K-12. Nucleic Acids Res. 2019;47: D212–D220.
745   doi:10.1093/nar/gky1077

746

747   44. Bar-Even A, Paulsson J, Maheshri N, Carmi M, O'Shea E, Pilpel Y, et al. Noise in protein
748   expression scales with natural protein abundance. Nat Genet. 2006;38: 636–643.
749   doi:10.1038/ng1807

750

751   45. Hausser J, Mayo A, Keren L, Alon U. Central dogma rates and the trade-off between precision and
752   economy in gene expression. Nat Commun. 2019;10: 1–15. doi:10.1038/s41467-018-07391-8

753

754   46. Lagarias JC, Reeds JA, Wright MH, Wright PE. Convergence Properties of the Nelder--Mead
755   Simplex Method in Low Dimensions. SIAM J Optim. 1998;9: 112–147.
756   doi:10.1137/S1052623496303470

757

758   47. Maurizi MR. Proteases and protein degradation in Escherichia coli. Experientia. 1992;48: 178–201.
759   doi:10.1007/BF01923511

760

761   48. Koch AL, Levy HR. Protein turnover in growing cultures of Escherichia coli. J Biol Chem. 1955;217:
762   947–957. Available: https://www.ncbi.nlm.nih.gov/pubmed/13271454

763

764   49. Rydenfelt M, Garcia HG, Cox RS 3rd, Phillips R. The influence of promoter architectures and
765   regulatory motifs on gene expression in Escherichia coli. PLoS One. 2014;9: e114347.
766   doi:10.1371/journal.pone.0114347

767

768   50. Buchler NE, Gerland U, Hwa T. On schemes of combinatorial transcription logic. Proc Natl Acad
769   Sci U S A. 2003;100: 5136–5141. doi:10.1073/pnas.0930314100

770

771   51. Golding I, Paulsson J, Zawilski SM, Cox EC. Real-Time Kinetics of Gene Activity in Individual
772   Bacteria. Cell. 2005;123: 1025–1036. doi:10.1016/j.cell.2005.09.031

773

774   52. Startceva S, Kandavalli VK, Visa A, Ribeiro AS. Regulation of asymmetries in the kinetics and
775   protein numbers of bacterial gene expression. Biochimica et Biophysica Acta (BBA) - Gene
776   Regulatory Mechanisms. 2019;1862: 119–128. doi:10.1016/j.bbagrm.2018.12.005

777

778   53. Rhee KY, Opel M, Ito E, Hung S p., Arfin SM, Hatfield GW. Transcriptional coupling between the
779   divergent promoters of a prototypic LysR-type regulatory system, the ilvYC operon of Escherichia
780   coli. Proc Natl Acad Sci U S A. 1999;96: 14294–14299. doi:10.1073/pnas.96.25.14294
781

782   54. Jia J, King JE, Goldrick MC, Aldawood E, Roberts IS. Three tandem promoters, together with IHF,
783   regulate growth phase dependent expression of the Escherichia coli kps capsule gene cluster. Sci
784   Rep. 2017;7: 1–11. doi:10.1038/s41598-017-17891-0
785
786   55. Yeung E, Dy AJ, Martin KB, Ng AH, Del Vecchio D, Beck JL, et al. Biophysical Constraints Arising
787   from Compositional Context in Synthetic Gene Networks. Cell Syst. 2017;5: 11-24.e12.
788   doi:10.1016/j.cels.2017.06.001
789
790   56. Chong S, Chen C, Ge H, Xie XS. Mechanism of transcriptional bursting in bacteria. Cell. 2014;158:
791   314–326. doi:10.1016/j.cell.2014.05.038
792
793   57. Epshtein V, Nudler E. Cooperation between RNA polymerase molecules in transcription
794   elongation. Science. 2003;300: 801–805. doi:10.1126/science.1083219
795
796   58. Li M, Wang J, Geng Y, Li Y, Wang Q, Liang Q, et al. A strategy of gene overexpression based on
797   tandem repetitive promoters in Escherichia coli. Microb Cell Fact. 2012;11: 19. doi:10.1186/1475-
798   2859-11-19
799
800   59. Chauhan V, Bahrudeen MNM, Palma CSD, Ines SCB, Almeida BLB, Dash S, et al. Analytical
801   kinetic model of native tandem promoters in E. coli, Dryad, Dataset. doi: 10.5061/dryad.bnzs7h4b

802